

## Percolation of Fortuin-Kasteleyn clusters for the random-bond Ising model

Hauke Fajen,<sup>1</sup> Alexander K. Hartmann<sup>1,\*</sup> and A. P. Young<sup>2</sup>

<sup>1</sup>*Institut für Physik, Universität Oldenburg, 26111 Oldenburg, Germany*

<sup>2</sup>*Physics Department, University of California Santa Cruz, Santa Cruz, California 95064, USA*



(Received 4 June 2020; accepted 24 June 2020; published 13 July 2020)

We apply generalizations of the Swendson-Wang and Wolff cluster algorithms, which are based on the construction of Fortuin-Kasteleyn clusters, to the three-dimensional  $\pm 1$  random-bond Ising model. The behavior of the model is determined by the temperature  $T$  and the concentration  $p$  of negative (antiferromagnetic) bonds. The ground state is ferromagnetic for  $0 \leq p < p_c$ , and a spin glass for  $p_c < p \leq 0.5$  where  $p_c \simeq 0.222$ . We investigate the percolation transition of the Fortuin-Kasteleyn clusters as a function of temperature for large system sizes up to  $N = 200^3$  spins. Except for  $p = 0$  the Fortuin-Kasteleyn percolation transition occurs at a higher temperature than the magnetic ordering temperature. This was known before for  $p = \frac{1}{2}$  but here we provide evidence for a difference in transition temperatures even for  $p$  arbitrarily small. Furthermore, for all values of  $p > 0$ , our data suggest that the percolation transition is universal, irrespective of whether the ground state exhibits ferromagnetic or spin-glass order, and is in the universality class of standard percolation. This shows that correlations in the bond occupancy of the Fortuin-Kasteleyn clusters are irrelevant, except for  $p = 0$  where the clusters are strictly tied to Ising correlations so the percolation transition is in the Ising universality class.

DOI: [10.1103/PhysRevE.102.012131](https://doi.org/10.1103/PhysRevE.102.012131)

### I. INTRODUCTION

Magnetic systems with quenched disorder, such as spin glasses (SGs) [1–4] and random-field systems, exhibit phase transitions between low-temperature-ordered and high-temperature-disordered (paramagnetic) phases in high enough dimensions. This is similar to the case of pure systems like ferromagnets [5] but spin glasses in particular exhibit a much richer behavior and many aspects of the low-temperature phase are still not well understood. Since most disordered models cannot be solved analytically, one has to resort to computer simulations [6]. For the special case of zero temperature, there are often efficient algorithms [7]. However, for systems coupled to a heat bath at finite temperature, Monte Carlo simulations [8,9] are generally used. For the *pure* Ising model, efficient cluster Monte Carlo (MC) approaches exist [10,11], which are based on the construction of Fortuin-Kasteleyn (FK) [12] clusters of spins. This gives fast equilibration even close to the phase transition point. The reason is that the FK clusters percolate [13] *precisely* at the phase transition [14].

It is also possible to implement cluster MC algorithms like the Wolff algorithm for spin glasses, but unfortunately these are not efficient because, in the vicinity of the spin-glass phase transition, each update flips almost all the spins [15]. The reason is that percolation of the FK clusters happens at a much higher temperature than the magnetic-ordering phase transition temperature [16]. Other approaches for cluster algorithms for spin glasses have been tried [17–21]. Nevertheless, the largest system treated in the most recent application [21] exhibits just  $N = 12^3$  spins. Hence, so far, no algorithm turned out to be efficient enough to equilibrate three-dimensional

standard spin glasses and related models of considerable size. Nevertheless, single-spin-flip algorithms are still used for studying spin glasses numerically. Some improvement is obtained by using parallel tempering [22,23], and by running parallel tempering on a special-purpose high-performance computer “JANUS” [24]. By this combination it has been possible to simulate an  $N = 48^3$  spin-glass model near the transition temperature.

When just concentrating on the percolation properties, spin glasses have been investigated also with respect to other types of clusters, such as the two-replica FK (TRFK) approach [25] and Chayes-Machta-Redner (CMR) clusters [26,27]. For these two types of clusters, percolation transitions have been found [28] by simulating and analyzing three-dimensional spin glasses in equilibrium up to size  $N = 12^3$ . For the CMR clusters, the transition seems to be very close to that of the standard FK clusters. For the TRFK clusters, the transition appears at much lower temperatures, but still well above  $T_c$ .

In order to obtain a better understanding of the nature of standard FK clusters and their percolation transitions, as well as algorithmic efficiency, we study here the  $\pm 1$  random-bond Ising model [29], which is a particular case of the standard spin glass. It consists of  $N$  Ising spins  $\sigma_i = \pm 1$  placed on a  $d$ -dimensional hypercubic lattice of linear size  $L$ , i.e.,  $N = L^d$ . The Hamiltonian is given by

$$H = - \sum_{(i,j)} J_{ij} \sigma_i \sigma_j. \quad (1)$$

Each spin  $i$  interacts with its nearest neighbors  $j$  via an interaction which is a quenched random variable  $J_{ij}$ . Here, we use a bimodal distribution so each bond is anti-ferromagnetic ( $J_{ij} = -1$ ) with probability  $p$  and ferromagnetic ( $J_{ij} = +1$ ) with probability  $1 - p$ . As usual for quenched disorder, the

\*a.hartmann@uni-oldenburg.de

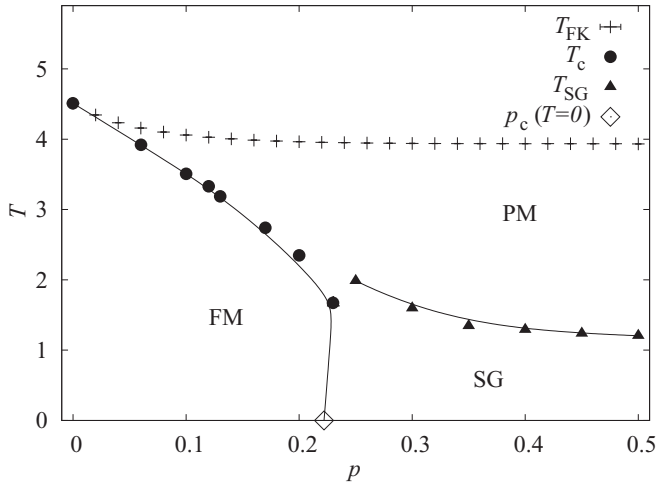


FIG. 1. Phase diagram showing the line of percolation transitions of the FK clusters, and the lines of phase transitions between ferromagnetic (FM), paramagnetic (PM), and spin-glass (SG) phases. Lines are guides for the eyes only. The data for the ferromagnetic transition temperature  $T_c(p)$ , shown as filled circles, are from Ref. [31], the data for the spin-glass transition temperature  $T_{SG}$ , shown as filled triangles, are from Ref. [30], and the value  $p_c(T=0)$  where the spin glass and ferromagnetic phases meet at  $T=0$ , shown as open diamond symbol, is from Ref. [32]. The data for the percolation transition temperature  $T_{FK}(p)$ , shown as plus symbols, are from this work.

result of any measurement will depend on the realization of the disorder, so one has to perform an average over many realizations of disorder in addition to doing the thermal average.

We consider here the case of a simple cubic lattice for which the low-temperature phase is ferromagnetic for a small concentration ( $p$ ) of antiferromagnetic bonds and a spin glass for a larger concentration. We denote the paramagnet to ferromagnet transition temperature by  $T_c(p)$  and the paramagnet to spin-glass transition by  $T_{SG}(p)$ . The phase diagram in the  $p$ - $T$  plane has been determined by Monte Carlo simulations [30,31] (see Fig. 1). For  $T=0$  the transition point between the ferromagnetic and spin-glass phases was found [32] to be approximately  $p_c = 0.222(5)$ .

In this study, we investigate the behavior of FK clusters and, related to this, the performance of the Wolff algorithm, in the  $p$ - $T$  plane. We are interested only in the vicinity of the percolation transition of FK clusters, where the Wolff algorithm is efficient and so we can equilibrate large system sizes up to  $N = 200^3$  spins. We know that for the pure ( $p=0$ ) ferromagnet, the FK percolation transition coincides with the ferromagnet-paramagnet transition, and here we investigate whether this is true for any other values of  $p$ . Results of some test simulations performed previously [31] suggest this is not the case, at least for some values of  $p$  in the ferromagnetic regime. One still needs to investigate whether the Wolff algorithm performs much better than parallel tempering in the region of the spin-glass phase close to the ferromagnetic phase because the fraction  $1 - c_p = 1 - 4[p^3(1-p) + p(1-p)^3]$  of nonfrustrated plaques [33] is smaller than  $\frac{1}{2}$ , which might allow for the existence of large connected clusters of nonfrustrated plaquettes, where the Wolff algorithm could operate

successfully. In addition to the performance of the Wolff algorithm, our main interest in this work is to investigate how the FK percolation transition changes as a function of  $p$ .

We present an extensive study of the FK percolation transition in the full range of interest  $0 \leq p \leq \frac{1}{2}$ , finding that this transition happens above the phase transition line for all  $p > 0$ . Only for the pure ferromagnet,  $p=0$ , does it coincide with the FM-PM transition. In addition, the critical exponents seem to be those of the (uncorrelated) percolation problem everywhere along the FK transition percolation transition line, including both the ferromagnetic and spin-glass regions (see Fig. 1). The only exception is for  $p$  precisely equal to 0, the pure ferromagnet, for which the critical exponents are those of the Ising model. Finally, our result indicates that in the spin-glass region close to  $p_c$  the Wolff algorithm does not perform notably better than for the standard ( $p = \frac{1}{2}$ ) spin-glass case.

Our paper is organized as follows. In Sec. II, we review the algorithms we used. Next, in Sec. III, we present our results, and finally in Sec. IV we give a summary and discussion.

## II. METHODS

To study the FK percolation transition and to investigate the efficiency of the Wolff algorithm we construct FK clusters at each step as follows:

(i) Bonds where  $J_{i,j}\sigma_i\sigma_j > 0$  are said to be *satisfied*, and we *activate* them with probability  $p_{\text{act}} = 1 - e^{-2\beta|J_{ij}|}$ . Unsatisfied bonds are never activated.

(ii) We determine all clusters of spins connected by activated bonds, as in bond percolation.

A cluster is said to be *wrapping* or *percolating* if it spans the lattice between the periodic boundaries and so is connected back to itself. For each step, we record whether a cluster is wrapping (this is typically the largest one), and we also monitor the sizes of all clusters to investigate the distribution of cluster sizes. Finally, we generate the next configuration according to the Wolff algorithm by selecting a spin at random and flipping the spins (with “acceptance probability” one) in the cluster which contains it.

Averages are done both over the spin configurations for a given realization and a disorder average over a large number of different realizations; we typically considered 1000 realizations. The quantities that we measure are as follows:

- (1) The average wrapping probability  $p_{\text{wrap}}$ .
- (2) The fraction of sites in the largest cluster  $P$ .
- (3) The number  $n_s$  of clusters of size  $s$ .
- (4) The average size  $S$  of the clusters excluding the largest one (this would be the percolating cluster in the percolating phase). The average is done with respect to all sites, i.e.,  $S = \sum_s s^2 n_s / \sum_s s n_s$ .
- (5) The average size of the flipped clusters  $n_{\text{Wolff}}$ .
- (6) The average size  $\langle s \rangle$  of a cluster with a radius  $R$ .

For high temperatures the activation probability  $p_{\text{act}}$  is small, leading to many small clusters which do not wrap. On the other hand, for low temperatures,  $p_{\text{act}}$  will be large leading to few clusters and typically one big wrapping cluster. Thus, in-between, there exists a percolation transition of the FK clusters at some temperature  $T_{FK}$ , such that, in the thermodynamic limit,  $N \rightarrow \infty$ , one finds  $p_{\text{wrap}} \rightarrow 0$  for  $T > T_{FK}$  and  $p_{\text{wrap}} \rightarrow 1$  for  $T < T_{FK}$ .

We analyze our data using finite-size scaling (FSS), as is standard in percolation transitions [13]. According to FSS, at a second-order percolation transition near the critical point, the wrapping probability should exhibit a scaling behavior

$$p_{\text{wrap}}(L, T) = f_{\text{wrap}}((T - T_{\text{FK}})L^{1/\nu}), \quad (2)$$

where  $\nu$  is the critical exponent which describes the divergence of the correlation length of the FK clusters. Thus, the parameters  $T_{\text{FK}}$  and  $\nu$  can be determined by varying them until the data for different system sizes collapse on to the same universal curve  $f_{\text{wrap}}(\tilde{x})$ .

Furthermore, in the percolating phase, the fraction of sites in the largest (i.e., percolating) cluster in an infinite system goes to zero like  $P \sim (T_{\text{FK}} - T)^\beta$  as  $T$  approaches  $T_{\text{FK}}$  from below. For a finite system, this becomes, according to FSS,

$$P(L, T) = L^{-\beta/\nu} f_P((T - T_{\text{FK}})L^{1/\nu}), \quad (3)$$

allowing us to obtain the critical exponent  $\beta$ . The average cluster size behaves in a similar way, as described by the finite-size scaling relation

$$S(L, T) = L^{\gamma/\nu} f_S((T - T_{\text{FK}})L^{1/\nu}), \quad (4)$$

where  $\gamma$  is the exponent describing the divergence of the average cluster size of an infinite system  $S \sim (T - T_{\text{FK}})^{-\gamma}$ . Note that in computing  $S$  we neglect the largest cluster, so  $S$  has a maximum near the percolation transition because in the nonpercolating phase there are only many small clusters, while in the percolating phase most sites belong to the percolating cluster which is neglected. Thus, the scaling function  $f_S$  exhibits a peak at some value  $x_{\text{peak}}$ , corresponding to a temperature  $T_{\text{peak}} = T_{\text{FK}} + x_{\text{peak}}L^{-1/\nu}$ , which means that the height of  $S^*$  at the peak scales with a power law

$$S^* \sim L^{\gamma/\nu}, \quad (5)$$

allowing us to obtain the critical exponent  $\gamma$ .

Also, the distribution  $n_s$  of cluster sizes has similar behavior when considering how it changes near the critical point. The only difference is that it is not the system size, but rather the cluster size, which enters explicitly:

$$n_s(s, T) = s^{-\tau} f_n((T - T_{\text{FK}})s^\sigma), \quad (6)$$

defining the critical exponents  $\tau$  and  $\sigma$ . That means that the distribution  $n_s$  of cluster sizes at the critical point  $T_{\text{FK}}$ , for an infinite system but approximately also for a finite system, is expected to follow a power law

$$n_s(T_{\text{FK}}) \sim s^{-\tau}. \quad (7)$$

Finally, all nonpercolating clusters have a fractal structure: the cluster size  $s$  scales with the cluster radius  $R$  with

$$s \sim R^{d_f}, \quad (8)$$

where  $d_f$  is the fractal dimension, and the cluster radius  $R$  is defined as

$$R_s^2 = \sum_{i=1}^s \frac{|\vec{r}_i - \vec{r}_c|^2}{s}. \quad (9)$$

Here,  $\vec{r}_c$  is the center of mass of the cluster that is calculated, to cope with the periodic boundary conditions, by mapping

every coordinate onto a circle [34], calculating the center of mass of this circle, and mapping the result back.

The critical exponents are not independent of each other. Instead, they are connected through scaling relations, such that there are only two independent exponents. The scaling relations for the standard percolation problem are often expressed [13] as

$$\tau = \frac{d}{d_f} + 1, \quad \gamma = \frac{3 - \tau}{\sigma}, \quad \beta = \nu(d - d_f). \quad (10)$$

We will verify that our computed values for  $\nu$ ,  $\tau$ ,  $\gamma$ ,  $d_f$ ,  $\sigma$ , and  $\beta$  obey these relations.

### III. RESULTS

We performed simulations for various values of  $p \in [0, 0.5]$ . For each value of  $p$  we treated different system sizes  $L \in [10, 100]$ , and for a few values of  $p$  we also did simulations for  $L = 200$  (see below). All results are disorder averages over typically 1000 realizations, with the exception of some cases where a few runs were not completed on our cluster due to technical reasons (there were always more than 960 realizations).

For each realization we performed Monte Carlo simulations using the Wolff algorithm for 72 temperatures equally spaced in [3.615, 4.68], i.e., with spacing  $\Delta T = 0.015$ . For the selected cases of  $p = 0.1, 0.3$ , and  $0.5$  (and also for  $p = 0$  as a comparison with other work and a check on our code), we studied 20 additional temperatures spaced by  $\Delta T = 0.003$  very close to  $T_{\text{FK}}$ , in order to determine the critical properties precisely.

To check for equilibration we averaged over intervals  $[t/2, t]$  for a logarithmically increasing set of times  $t$ , and required that there is no systematic trend for the last several values of  $t$ . Typically, near the FK percolation transition which is the region we are interested in, equilibration is achieved within a few Wolff cluster steps. Note that near the percolation transition typically large clusters are flipped, thus, one or few Wolff cluster steps correspond roughly to one sweep of a traditional single-spin-flip algorithm. For small systems  $L \leq 30$ , we perform  $2 \times 10^5$  Wolff steps per realization, while for the larger systems, which run slower but still need only a few steps to equilibrate, we do  $5 \times 10^3$  steps.

To determine the position of the FK percolation transitions, we monitor the wrapping probability of the FK clusters. An example is shown for  $p = 0.1$  in the inset of Fig. 2. A clear decrease of the wrapping probability beyond  $T \approx 4$  is visible. We performed a data collapse according to Eq. (2) near the phase transition point, as shown in the main plot of Fig. 2, to determine  $T_{\text{FK}}$  and the critical exponent  $\nu$  of the correlation length, resulting in  $T_{\text{FK}} = 4.060(3)$  and  $\nu = 0.9(1)$ . The best-fit parameters were determined from the method discussed in the Appendix of Ref. [35] and in Ref. [36]. Note that to avoid a strong influence of finite-size corrections we did not use all available data for the collapse, but restricted ourselves to system sizes  $L > 20$  and the vicinity  $(T - T_{\text{FK}})L^{1/\nu} \in [-2.125, 0.5]$  of the phase transition. This small fitting range was necessary to reproduce very accurately the literature value for the  $p = 0$  pure ferromagnetic case, even though the data collapse is

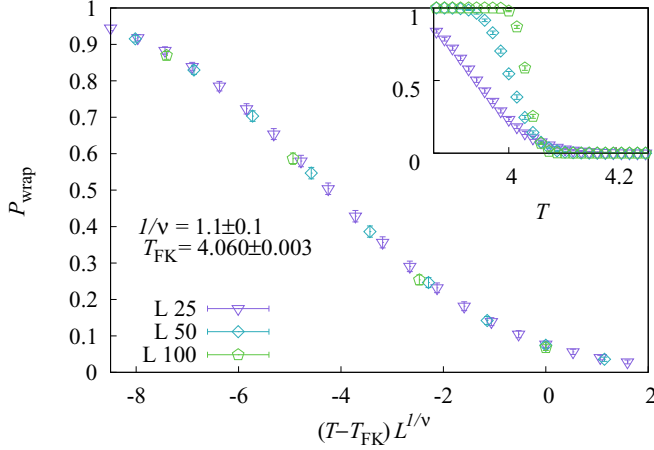


FIG. 2. Wrapping probability as function of temperature  $T$  for  $p = 0.1$ , for various system sizes  $L$ . The inset shows the raw data, while in the main plot a data collapse to determine  $T_{\text{FK}}$  and  $\nu$  gives  $1/\nu = 1.1(1)$  and  $T_{\text{FK}} = 4.060(3)$ .

visually very good for a much larger range. See also the discussion of systematic errors below.

In a similar way, we analyzed the data for other values of  $p$ . The resulting values of  $T_{\text{FK}}$  as a function of  $p$  are shown in the phase diagram in Fig. 1, along with the values for the FM-PM and SG-PM phase transitions obtained from the literature [30,31], and the critical concentration  $p_c$  for the zero-temperature FM-SG transition [32]. Interestingly, the FK percolation transition seems to coincide with magnetic-ordering transition only for the pure ferromagnetic system ( $p = 0$ ). For all other values of  $p$ ,  $T_c < T_{\text{FK}}$  even close to the pure ferromagnet. Hence, even if the ground state is ferromagnetic, i.e., for  $0 < p < p_c$ , the FM-PM phase transition cannot be understood as a percolation transition of the FK clusters.

The resulting values of  $\nu$  as a function of  $p$  are shown in Fig. 3. For  $p = 0$ , we recover the literature value for the pure Ising ferromagnet [37], but with larger error bars (which is natural, because our main numerical effort goes into the necessary disorder average and considering several values of  $p$ ). For all other values of  $p$ , including both ferromagnetic and spin-glass regions, we find that  $\nu$  is compatible with the previously found [16] value of  $\nu = 0.88(5)$ . Note that a majority of values we found are systematically a bit larger than the literature value. By extending the collapse interval (on the  $T$  axis) beyond the range  $[-2.125, 0.5]$ , we observe for almost all values of  $p$  a systematic upshift by about 0.02, i.e., an even stronger deviation. Thus, by going to larger sizes or including corrections to scaling into the data-collapse approach, we would arrive at more precise results. Nevertheless, since the focus of our work is the general study of the model along the  $p$  axis, not the determination of precise exponent values (which would require much more than the already large computational effort), we do not go into details here. Anyway, our results are also compatible with the value [38] for the standard percolation problem, in which there are no correlations between the occupancies of the bonds. By contrast, in FK clusters there *are* correlations for all  $p$  but interestingly they do not seem to affect the critical behavior,

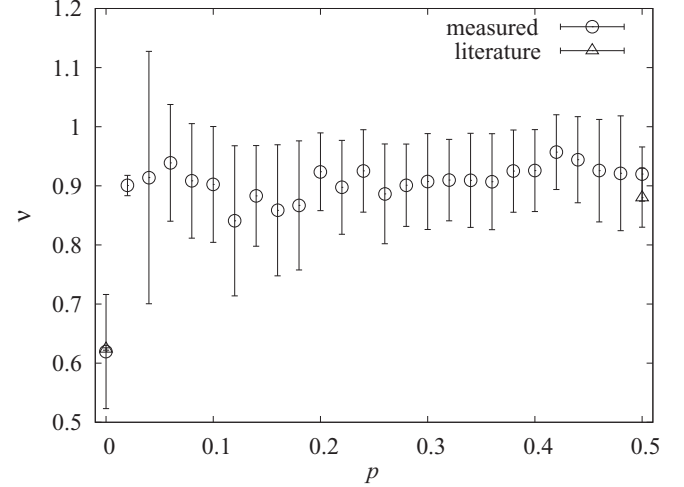


FIG. 3. The critical exponent  $\nu$  as a function of  $p$ . The value of  $\nu$  for  $p = 0$  is from Ref. [37] and the value for  $p = 0.5$  indicated by a triangle is from Ref. [16]. Note that for the case  $p = 0.02$  the error bar is very small. The reason is that within the fitting window (see text) there are very few data points for this value of  $p$ , which leads to close to overfitting. We could use smaller sizes here, which increases the error bar, but we prefer to use the same fitting conditions for all values of  $p$ .

except for  $p = 0$  where the bond occupancies are *rigorously constrained* to follow Ising correlations.

To investigate universality more carefully we have evaluated the other critical exponents with additional data near  $T_{\text{FK}}$  for the values  $p = 0$  (for a consistency check),  $p = 0.1$  (a ferromagnetic case),  $p = 0.3$ , and  $p = 0.5$  (SG cases; for the latter value the critical behavior of the FK percolation clusters is already partially known [16]).

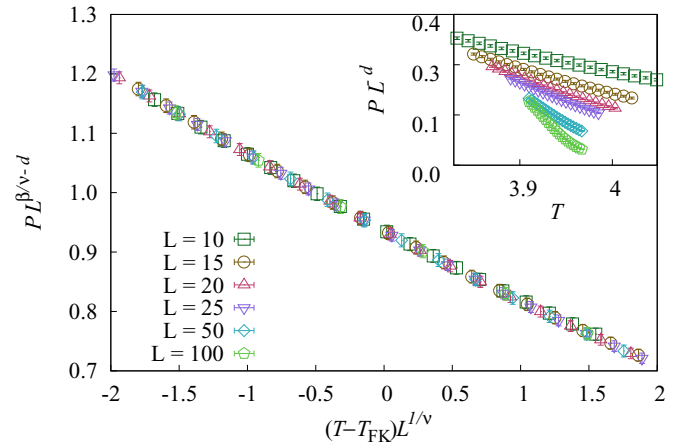


FIG. 4. The fraction of sites in the infinite cluster  $P$  as a function of the temperature  $T$  in the vicinity of  $T_{\text{FK}}$ , for  $p = 0.3$  and various system sizes  $L$ . The inset shows the raw data, while the main plot shows the data rescaled according to Eq. (3), with best-fitting values  $\beta = 0.413(9)$ ,  $\nu = 0.87(2)$ , and  $T_{\text{FK}} = 3.93858(7)$ . Note that these values are not the same as those in Table I because the values shown here are specific-case results, while the table shows final estimates arising from summarizing different approaches, including an estimate of systematic errors.

TABLE I. Best estimates for the critical temperatures  $T_{\text{FK}}$  and critical exponents  $\nu$ ,  $\tau$ ,  $\gamma$ , and  $\beta$ . The numbers in parentheses denote the error bars in the last digit. Also shown are the values for  $\tau$ ,  $\gamma$ , and  $\beta$  obtained by inserting the values for  $\nu$ ,  $d_f$ ,  $\tau$ , and  $\sigma$  into the scaling relations in Eq. (10).

$p$	$T_{\text{FK}}$	$\nu$	$\tau$	$\gamma$	$\beta$	$\sigma$	$d_f$	$\tau = \frac{d}{d_f} + 1$	$\gamma = \frac{3-\tau}{\sigma}$	$\beta = \nu(d - d_f)$
0.0	4.5112(5)	0.65(2)	2.20(4)	1.2(1)	0.313(5)	0.69(1)	2.49(6)	2.20(3)	1.16(8)	0.33(5)
0.1	4.0584(3)	0.871(6)	2.189(5)	1.75(5)	0.417(1)	0.41(1)	2.52(4)	2.19(2)	1.98(6)	0.42(4)
0.3	3.9386(5)	0.87(2)	2.199(5)	1.7(1)	0.413(9)	0.44(2)	2.52(4)	2.19(2)	1.82(9)	0.42(5)
0.5	3.934(3)	0.87(3)	2.20(2)	1.7(1)	0.41(1)	0.43(1)	2.53(3)	2.19(1)	1.87(9)	0.41(4)

For the fraction of sites in the infinite cluster (the order parameter), we show data for  $p = 0.3$  in Fig. 4. From a finite-size scaling collapse of the data we obtain the best-fitting parameters  $\beta = 0.413(9)$ ,  $\nu = 0.87(2)$ , and  $T_{\text{FK}} = 3.93858(7)$ . The errors were determined such that they take the correlations between the different estimates into account. Following Refs. [39,40], we determined the covariance matrix between the estimates of  $\beta$ ,  $\nu$ , and  $T_{\text{FK}}$  by bootstrapping. This means we generate bootstrap samples of the original data and (automatically) perform the data collapse on each bootstrap sample. Typically, we generate 100 bootstrap samples and so get 100 different estimates, from which the covariance matrix can be determined. The resulting covariance matrices, for four values of  $p$ , are shown in Table II in the Appendix. After inversion of the covariance matrix, the error can be obtained from its entries and suitable normalization [39].

The bootstrap approach only gives the statistical errors. In order to estimate the systematic errors, we reduced the interval (on the  $T$  axis) where the data collapse is performed by a factor of 0.5 and obtain another set of estimates for the critical exponents. The difference between the estimates for the original collapse interval and the reduced one gives us a hint on the magnitude of systematic error contributions, which turned out to be significantly larger than the statistical error bars. The combination of systematic and statistic errors leads to  $\sigma(\beta) = 9 \times 10^{-3}$ ,  $\sigma(\nu) = 2 \times 10^{-2}$ , and  $\sigma(T_{\text{FK}}) = 5 \times 10^{-4}$  ( $p = 0.3$ ). The result for this and the other intensively studied cases are shown in Table I. Note that for  $T_{\text{FK}}$  and  $\nu$ , we have two independent estimates available, the other estimate coming from the percolation probability (see, e.g., Fig. 2). They are here assumed to be uncorrelated since they were obtained using independent simulations for different realizations of the disorder. For these two quantities we obtain the final estimates by using a weighted average ( $\bar{x} = \sum_i a_i x_i / \sum_j a_j$ ;  $x = T_{\text{FK}}$  and  $x = \nu$ ) with  $a_i = \frac{1}{\sigma(x_i)^2}$  as weights. The error of the combined value is then calculated using  $\sigma^2(\bar{x}) = (\sum_i \frac{1}{\sigma^2(x_i)})^{-1}$ .

In addition to the order parameter, we have also analyzed the data for the average cluster size  $S$ . As example, we show the result for  $p = 0.1$  and size  $L = 50$  as a function of temperature  $T$  in Fig. 5. The data exhibit a peak at some point ( $T^*$ ,  $S^*$ ). One can read off the critical exponent  $\gamma$  from the  $L^{\gamma/\nu}$  scaling [see Eq. (5)] of the peak height as a function of  $L$ . The data are shown in the inset of Fig. 5, the fit to the power-law results in  $\gamma/\nu = 2.005(4)$ . We estimated the systematic contributions to the error bar by varying the fitting range a bit (excluding the smallest and the largest sizes, respectively), resulting in a larger error bar of 0.04. The final results for  $\gamma$ ,

also for other values of  $p$  which have been studied in detail, are shown in Table I. Again, we observe that for  $p > 0$  the results agree with each other.

To obtain the critical exponent  $\tau$ , we analyze the distribution of cluster sizes, excluding the largest cluster, at the critical point for a rather large system size  $L = 200$ . As an example, we present our results for  $p = 0.3$  in Fig. 6. The data exhibit a high quality which allows us to observe a power law over about 10 decades in probability. A power-law fit according to Eq. (7) gives  $\tau = 2.199(5)$ . This value, and the results for the three other selected cases, are also shown in Table I. The results we have found for all values of  $p > 0$  are compatible with the values for standard percolation in three dimensions.

To further verify the critical exponent  $\sigma$ , we also determined the distribution of cluster sizes away from the critical temperature, and the data for  $p = 0.3$  is shown in Fig. 7 for  $L = 150$ . Since the automatic fitting program did not converge well, we did the data-collapse analysis visually, obtaining  $\sigma = 0.44(2)$ . For  $\tau$  and  $T_{\text{FK}}$ , we used the values found in the earlier analysis which are given in Table I.

Another critical exponent that we obtained is the fractal dimension  $d_f$ . Here, we looked at the average cluster size  $\langle s \rangle$  as a function of the radius  $R$  of the cluster. Figure 8 shows an example of such a dependency for  $p = 0.1$ . It is clear that data grow like a power law, except for big values of  $R$  where the

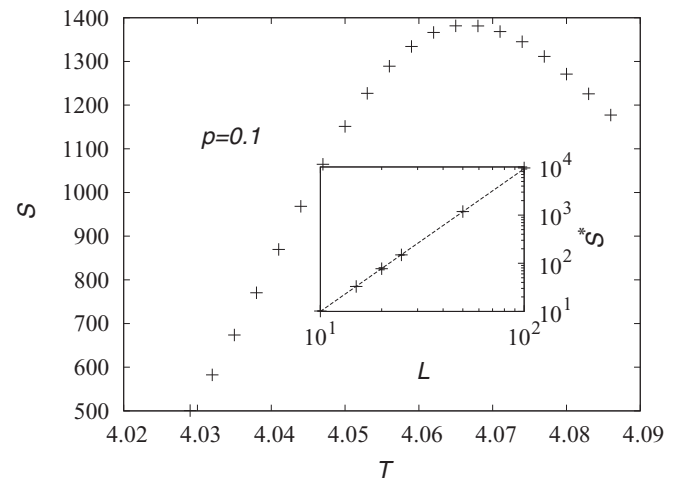


FIG. 5. Average cluster size  $S$  at  $L = 50$  and  $p = 0.1$  as a function of temperature  $T$ , near the FK percolation transition  $T_{\text{FK}}$ . The data exhibit a peak with peak height  $S^*$ . The inset shows the peak height as function of  $L$ . The line in the inset shows the result of a fit to Eq. (5) resulting in  $\gamma/\nu = 2.005(4)$ .

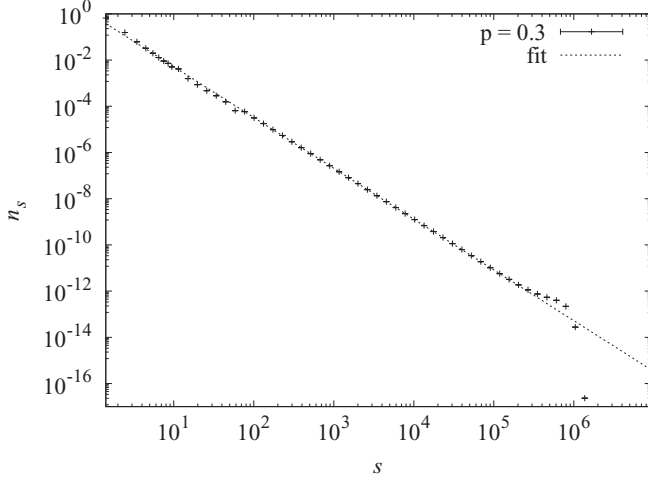


FIG. 6. Cluster size distribution at the critical temperature for  $p = 0.3$  with a system size of  $N = 200^3$ . Fitting to Eq. (7) gives  $\tau = 2.199 \pm 0.005$ .

size of the system limits the size of the clusters. From fitting to the power law (8) we obtained an exponent  $d_f = 2.52(4)$ , where the error bar includes also an estimate of the systematic error, obtained by varying the fitting range.

The exponents should obey the scaling relations in Eq. (10). The values obtained when inserting the measured values for  $\nu$ ,  $d_f$ ,  $\sigma$ , and  $\tau$  from Table I to estimate  $\tau$ ,  $\gamma$ , and  $\beta$  from the scaling relations are shown in the last three columns in Table I. Almost all these values are compatible with the directly measured values within error bars. Only for the case  $p = 0.1$ , does our estimate for  $\gamma$  differ from that obtained from scaling relation by more than two  $\sigma$ . Since this will happen in about 5% of all cases in Gaussian statistics, we consider this one small outlier as being reasonable. Apart from one case where they are almost equal, the error bars from the scaling relations are larger than the error bars of the directly measured exponents due to error propagation.

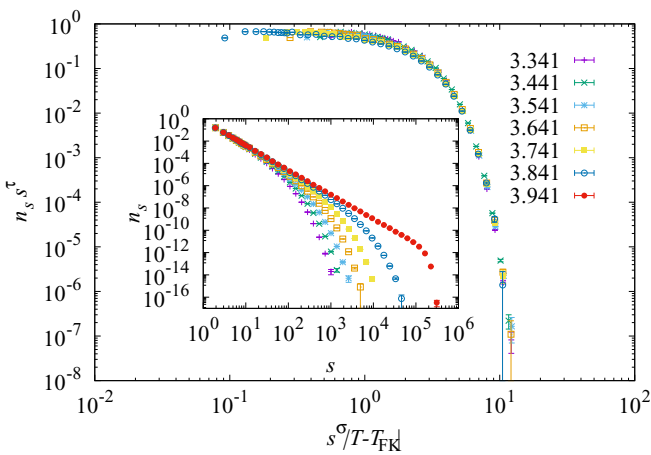


FIG. 7. Cluster size distribution at  $p = 0.3$  with a system size of  $N = 150^3$  at different temperatures. Except for the last temperature, which is above but close to  $T_{FK}$ , all the temperature values are smaller than  $T_{FK}$ . The inset shows the raw data, while the main plot shows rescaling according to Eq. (6).

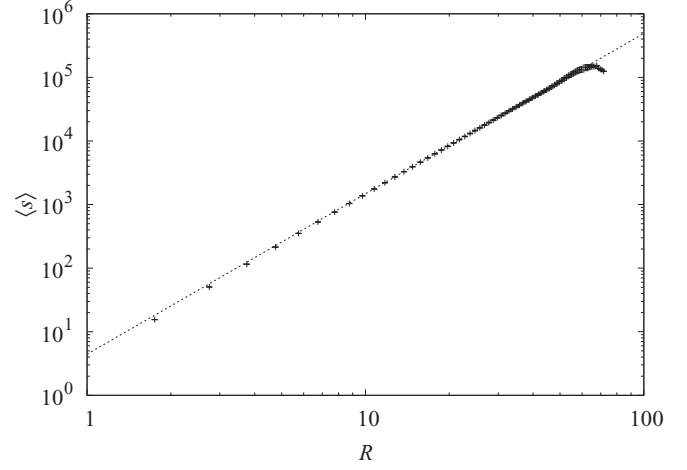


FIG. 8. The average cluster sizes  $\langle s \rangle$  as a function of the cluster radius  $R$  for  $p = 0.1$ . The line shows a fit to Eq. (8), resulting in an exponent  $d_f = 2.52(4)$ , where the error bar includes also an estimate of the systematic error, obtained by varying the fitting range.

Finally, we consider the question of whether the Wolff algorithm might be more efficient in the spin-glass phase near the FM-SG transition, i.e., for  $p$  just slightly greater than  $p_c$ , rather than for  $p = \frac{1}{2}$ . In Fig. 9 we show the average “effective” size of the flipped cluster as a function of the temperature  $T$  for  $p = 0.25$  ( $> p_c$ ). By “effective” we mean that if the cluster of flipped spins is larger than half of the system size, then we take the number of spins which are not flipped. We see that the clusters which are flipped near the SG phase transition are very small. One could already expect this from the phase diagram in Fig. 1, which shows that, for  $p = 0.25$  the FK percolation transition is considerably above the critical temperature  $T_{SG}$ . Thus, applying the Wolff algorithm in the spin-glass phase but near the spin-glass-ferromagnet phase boundary will not lead to any improvement over the approach of parallel tempering, just as for the standard spin-glass model which has  $p = 0.5$ .

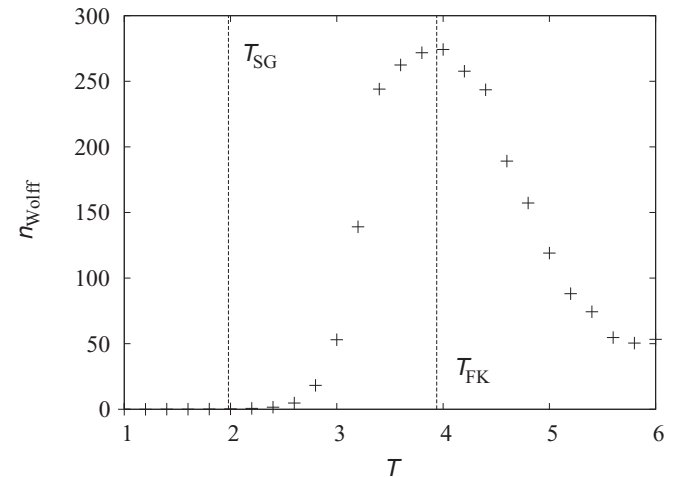


FIG. 9. Average size of the clusters flipped (or not flipped if this is smaller) by the Wolff algorithm as a function of temperature  $T$  for  $L = 10$  and  $p = 0.25$ .

## IV. SUMMARY

We have studied the percolation transitions of Fortuin-Kasteleyn clusters for the three-dimensional random-bond Ising model. Near the cluster percolation transition the Wolff algorithm can be used to efficiently sample equilibrium configurations. However, except for the pure Ising case ( $p = 0$ ), the temperature of the percolation transition is higher than that of the ferromagnet-paramagnet and spin-glass-paramagnet transitions, and for most values of  $p$  it is *much* higher (see Fig. 1). This renders the Wolff algorithm inefficient for the magnetic transitions except for  $p = 0$ . Indications of this behavior were already found in some test simulations of a previous study [31], where, for the FM-PM phase boundary at one value of  $p > 0$ , cluster algorithms were tried but turned out to be inefficient.

We have determined the critical exponents at the FK cluster percolation transition. For  $p = 0$ , the pure Ising case, we obtain the known values, which are those of the Ising model since the FK clusters are controlled by Ising correlations in this limit. For all other values  $0 < p \leq \frac{1}{2}$ , our results are compatible with the universal behavior of standard percolation, irrespective of whether the ground state exhibits ferromagnetic or spin-glass order. Since standard percolation has no correlations between the occupancy of the bonds, whereas bonds in the FK clusters *are* correlated, this implies that the correlations are irrelevant for universal properties, and so presumably are of short range for  $p > 0$ .

For future studies, it would be interesting to investigate other types of cluster algorithms [17,20,21] for the three-dimensional random-bond Ising model. So far, from the literature studies known to us, none of them turned out to be efficient enough to study the pure spin-glass case ( $p = \frac{1}{2}$ ) for large enough systems, but it could be that some will work well close to the FM-SG phase boundary or at least for ferromagnetic ordering of the random ( $p > 0$ ) case.

Finally, we feel it would be worthwhile to study the percolation properties of clusters constructed in a different way, for example, the two-replica cluster approach of by Machta, Newman, and Stein [28]. For the two variants of their model applied to the pure spin-glass case ( $p = 0.5$ ), they found the percolation transition to be slightly below, in the first case, and significantly below, in the second case, the percolation transition of the FK clusters, but still above  $T_c$ .

TABLE II. The covariance matrices for the data collapse for the fraction of sites in the infinite cluster as function of temperature. The matrices were obtained by bootstrapping (see the main text).

$p = 0$	$T_c$	$\frac{1}{\nu}$	$\frac{\beta}{\nu}$
$T_c$	$2.92 \times 10^8$	$3.62 \times 10^6$	$1.92 \times 10^6$
$\frac{1}{\nu}$	$3.62 \times 10^6$	$1.60 \times 10^3$	$5.24 \times 10^4$
$\frac{\beta}{\nu}$	$1.92 \times 10^6$	$5.24 \times 10^4$	$1.97 \times 10^4$
$p = 0.1$	$T_c$	$\frac{1}{\nu}$	$\frac{\beta}{\nu}$
$T_c$	$4.87 \times 10^9$	$2.16 \times 10^8$	$6.20 \times 10^8$
$\frac{1}{\nu}$	$2.16 \times 10^8$	$7.93 \times 10^7$	$4.06 \times 10^7$
$\frac{\beta}{\nu}$	$6.20 \times 10^8$	$4.06 \times 10^7$	$8.69 \times 10^7$
$p = 0.3$	$T_c$	$\frac{1}{\nu}$	$\frac{\beta}{\nu}$
$T_c$	$1.66 \times 10^9$	$-3.71 \times 10^9$	$1.42 \times 10^8$
$\frac{1}{\nu}$	$-3.71 \times 10^9$	$2.48 \times 10^6$	$2.65 \times 10^7$
$\frac{\beta}{\nu}$	$1.42 \times 10^8$	$2.65 \times 10^7$	$1.73 \times 10^7$
$p = 0.5$	$T_c$	$\frac{1}{\nu}$	$\frac{\beta}{\nu}$
$T_c$	$9.25 \times 10^8$	$4.59 \times 10^6$	$1.19 \times 10^6$
$\frac{1}{\nu}$	$4.59 \times 10^6$	$2.70 \times 10^4$	$6.48 \times 10^5$
$\frac{\beta}{\nu}$	$1.19 \times 10^6$	$6.48 \times 10^5$	$1.60 \times 10^5$

## ACKNOWLEDGMENTS

A.P.Y. thanks the Alexander von Humboldt Foundation for financial support through a Research Award. The simulations were performed at the HPC facilities GWDG Göttingen, HERO and CARL. HERO and CARL are both located at the University of Oldenburg (Germany) and funded by the DFG through its Major Research Instrumentation Programme (INST Grants No. 184/108-1 FUGG and No. 184/157-1 FUGG) and the No. Ministry of Science and Culture (MWK) of the Lower Saxony State.

## APPENDIX: COVARIANCE MATRIX

The covariance matrix between the estimates of  $T_c$ ,  $1/\nu$ , and  $\beta/\nu$ , obtained by performing the data collapse for around 100 bootstrap samples, is shown in Table II, for  $p = 0, 0.1, 0.3$ , and  $0.5$ .

[1] K. Binder and A. Young, *Rev. Mod. Phys.* **58**, 801 (1986).  
[2] M. Mézard, G. Parisi, and M. Virasoro, *Spin Glass Theory and Beyond* (World Scientific, Singapore, 1987).  
[3] *Spin Glasses and Random Fields*, edited by A. P. Young, 1st ed. (World Scientific, Singapore, 1998).  
[4] H. Nishimori, *Statistical Physics of Spin Glasses and Information Processing: An Introduction* (Oxford University Press, Oxford, 2001).  
[5] E. Ising, *Z. Phys.* **31**, 253 (1925).  
[6] A. K. Hartmann, *Big Practical Guide to Computer Simulations* (World Scientific, Singapore, 2015).

[7] A. K. Hartmann and H. Rieger, *Optimization Algorithms in Physics* (Wiley-VCH, Weinheim, 2001).  
[8] D. P. Landau and K. Binder, *Monte Carlo Simulations in Statistical Physics* (Cambridge University Press, Cambridge, 2000).  
[9] M. E. J. Newman and G. T. Barkema, *Monte Carlo Methods in Statistical Physics* (Clarendon, Oxford, 1999).  
[10] R. H. Swendsen and J.-S. Wang, *Phys. Rev. Lett.* **58**, 86 (1987).  
[11] U. Wolff, *Phys. Rev. Lett.* **62**, 361 (1989).  
[12] C. M. Fortuin and P. W. Kasteleyn, *Physica (Amsterdam)* **57**, 536 (1972).

- [13] D. Stauffer and A. Aharony, *Introduction To Percolation Theory* (CRC Press, Boca Raton, FL, 1994).
- [14] A. Coniglio and W. Klein, *J. Phys. A: Math. Gen.* **13**, 2775 (1980).
- [15] D. A. Kessler and M. Bretz, *Phys. Rev. B* **41**, 4778 (1990).
- [16] L. de Arcangelis, A. Coniglio, and F. Peruggi, *Europhys. Lett.* **14**, 515 (1991).
- [17] F. Niedermayer, *Phys. Rev. Lett.* **61**, 2026 (1988).
- [18] S. Liang, *Phys. Rev. Lett.* **69**, 2145 (1992).
- [19] J. Houdayer, *Eur. Phys. J. B* **22**, 479 (2001).
- [20] T. Jörg, *Progr. Theor. Phys. Suppl.* **157**, 349 (2005).
- [21] Z. Zhu, A. J. Ochoa, and H. G. Katzgraber, *Phys. Rev. Lett.* **115**, 077201 (2015).
- [22] C. Geyer, in *23rd Symposium on the Interface between Computing Science and Statistics* (Interface Foundation North America, Fairfax, VA, 1991), p. 156.
- [23] K. Hukushima and K. Nemoto, *J. Phys. Soc. Jpn.* **65**, 1604 (1996).
- [24] F. Belletti, M. Cotallo, A. Cruz, L. A. Fernandez, A. Gordillo-Guerrero, M. Guidetti, A. Maiorano, F. Mantovani, E. Marinari, V. Martin-Mayor, A. Muñoz-Sudupe, D. Navarro, G. Parisi, S. Perez-Gaviro, M. Rossi, J. J. Ruiz-Lorenzo, S. F. Schifano, D. Sciretti, A. Tarancon, R. Tripicciono *et al.*, *Comput. Sci. Eng.* **11**, 48 (2009).
- [25] C. M. Newman and D. L. Stein, Short-range spin glasses: Results and speculations, in *Spin Glasses*, edited by E. Bolthausen and A. Bovier (Springer, Berlin, 2007), pp. 159–175.
- [26] L. Chayes, J. Machta, and S. Redner, *J. Stat. Phys.* **93**, 17 (1998).
- [27] O. Redner, J. Machta, and L. F. Chayes, *Phys. Rev. E* **58**, 2749 (1998).
- [28] J. Machta, C. M. Newman, and D. L. Stein, *J. Stat. Phys.* **130**, 113 (2008).
- [29] S. Kirkpatrick, *Phys. Rev. B* **16**, 4630 (1977).
- [30] J. D. Reger and A. Zippelius, *Phys. Rev. Lett.* **57**, 3225 (1986).
- [31] M. Hasenbusch, F. Parisen Toldin, A. Pelissetto, and E. Vicari, *Phys. Rev. B* **76**, 094402 (2007).
- [32] A. K. Hartmann, *Phys. Rev. B* **59**, 3617 (1999).
- [33] J. Vannimenus and G. Toulouse, *J. Phys. C: Solid State Phys.* **10**, L537 (1977).
- [34] L. Bai and D. Breen, *J. Graphics Tools* **13**, 53 (2008).
- [35] J. Houdayer and A. K. Hartmann, *Phys. Rev. B* **70**, 014418 (2004).
- [36] O. Melchert, A program for automatic finite-size scaling analyses: A user's guide,, [arXiv:0910.5403v1](https://arxiv.org/abs/0910.5403v1) (2009).
- [37] C. F. Baillie, R. Gupta, K. A. Hawick, and G. S. Pawley, *Phys. Rev. B* **45**, 10438 (1992).
- [38] J. Wang, Z. Zhou, W. Zhang, T. M. Garoni, and Y. Deng, *Phys. Rev. E* **87**, 052107 (2013).
- [39] M. Weigel and W. Janke, *Phys. Rev. Lett.* **102**, 100601 (2009).
- [40] L. A. Fernández and V. Martin-Mayor, *Phys. Rev. E* **79**, 051109 (2009).